Statistical multistep direct calculations for (p,p') continuum spectra up to 200 MeV

W. A. Richter and A. A. Cowley
University of Stellenbosch, Stellenbosch 7600, South Africa

R. Lindsay
University of the Western Cape, Bellville 7530, South Africa

J. J. Lawrie, S. V. Förtsch, and J. V. Pilcher
National Accelerator Centre, Faure 7131, South Africa

R. Bonetti
Istituto di Fisica Generale Applicata dell'Università di Milano, Italy

P. E. Hodgson
Nuclear Physics Laboratory, Department of Physics, University of Oxford, Oxford OX1 3RH, United Kingdom
(Received 16 March 1992)

Double differential cross sections have been calculated for (p,p') reactions on ^{58}Ni, ^{100}Mo, and ^{197}Au targets at incident proton energies of 100, 120, 150, 175, and 200 MeV using the multistep direct nuclear reaction code of Bonetti and Chiesa, which is based on the statistical multistep direct theory of Feshbach, Kerman, and Koonin. Extensive comparisons are made with experimental data, and in general it is found that the theory gives a good description of the angular distributions. There is evidence that the predicted cross sections deviate more from experiment at very low and very high excitation energies of the residual nucleus. The effects of uncertainties in the input parameters of the theory are also considered, as well as possible ways to improve the accuracy of the implementation of the theory.

PACS number(s): 24.60.Gv, 25.40.−h

I. INTRODUCTION

Many theoretical models are available to interpret the continuum spectra of nucleon-induced inclusive reactions [1]. These models span the full range from classical formulations, such as the intranuclear cascade [2] model, to fully quantum-mechanical treatments, such as the statistical multistep reaction theory of Feshbach, Kerman, and Koonin (FKK) [3,4]. Recently, Koning and Akkermans [5] have presented a new leading-particle statistics theory of multistep direct reactions, from which the FKK model follows after some approximations. Furthermore, the relationship between the various quantum-mechanical theories and the semiclassical models, for example, the generalized exciton model, is clearly explained.

Apart from the intrinsic physics contained in the various theories, phenomenological simplifications are often introduced in the models for calculational convenience, and this may lead to further divergences between models which claim to include the same physics. Consequently, apart from the basics of a specific theory, the details of the way in which various simplifications are introduced in practical calculations are often very important.

Recently it has been shown [6,7,8] that the FKK theory can be successfully applied to predict direct-emission spectra of protons and neutrons induced by incident protons at energies above 100 MeV. The extracted strengths of the effective interactions have a reasonable incident-energy dependence. Consequently, it now becomes worthwhile to compare the FKK theory with an even wider range of experimental data above 100 MeV in order to investigate the variations with incident energy and target mass.

In this paper we present the results of statistical multistep direct- (MSD) emission calculations of the angular distributions for three targets at five different energies ranging from 100 to 200 MeV, and make detailed comparisons with experimental data. In view of the large body of data involved, and also the growing interest in preequilibrium phenomena, we aim to give a more comprehensive account of the systematics of the multistep direct calculations—the basic assumptions going into the theory used (the statistical multistep direct theory of Feshbach, Kerman, and Koonin), the various options available in a specific calculation, and the different factors which may influence the accuracy of such calculations.

Important factors to be considered include the following: (1) The level densities assumed, usually expressed in terms of a level density parameter a. (2) Multiparticle emission, which contributes to the experimental cross section but is not considered explicitly in the theory, e.g., quasifree knockout, and the emission of other particles such as deuterons and alphas. (3) Collective effects, which are prominent at low excitation energies in the residual nucleus. (4) Limitations on the excitation of a particle-hole pair in the first step (first encounter with a target nucleon) of the multistep process. (5) Sensitivity of

the calculations to the optical-model potential used. (6) The effect of distinguishing between neutrons and protons in the multistep chain. (7) The effect of other assumed forms for the two-body effective interaction. (8) Variations in the value of the effective interaction for the various steps. (9) Possible transitions between the multistep direct (P) and multistep compound (Q) chains in the preequilibrium sequential decay processes.

In Sec. II, some experimental details are discussed. The theory is presented and details of the calculations are described in Sec. III. Section IV A consists of a comparison between the theoretical and experimental angular distributions of the (p,p') continuum spectra at selected emission energies, and Sec. IV B describes the incident-energy and target-mass dependence of the extracted strength of the effective interaction. The sensitivity of the theoretical results with respect to the various factors listed above is considered in Secs. IV B and IV C. Conclusions regarding the emission- and incident-energy dependence of the various stages in the multistep chain and a comparison with a quasifree-knockout description of the first-step contribution are presented in Secs. IV D–IV F. Finally, in Sec. V, a summary of the main conclusions is given.

II. EXPERIMENTAL DETAILS

The experiment was performed at the cyclotron facility of the National Accelerator Centre, Faure. An account of the equipment has been presented in Ref. [9]. The data for ^{100}Mo were measured concurrently with those for ^{58}Ni and ^{197}Au, which have already been published [10,11]. Details of the techniques used and other procedures can also be found in Refs. [10,11].

The ^{100}Mo target was a self-supporting foil enriched to 96% in ^{100}Mo with a thickness of 1.19 ± 0.06 mg/cm^2 and a uniformity estimated to be better than 2%/mm. As for ^{58}Ni and ^{197}Au, the cross-section data for ^{100}Mo are also believed to be accurate to within a systematic error of 10%.

III. THEORY

A. The basic theory of Feshbach, Kerman, and Koonin

The FKK theory of multistep direct and multistep compound (MSC) emission has often been described [3]. We will give some of the expressions relevant to the discussion of the implementation of the MSD model. The basic assumptions of the theory are the following: the incoming particle interacts with a nucleon of the target nucleus by means of a two-body interaction. As a result, a particle is excited, and the residual nucleus is left in a one-particle–one-hole (1p-1h) state. Thus, one uses a microscopic description of the reaction, i.e., inelastic scattering, with the incident particle interacting with a neutron or proton in a shell-model orbital, and this target particle is then accepted into another shell-model orbital. Next it is assumed that the preequilibrium emission processes take place via successive particle-hole excitations of the nucleus which can only occur between the available energy levels in the nucleus.

The theory of direct reactions has proved very successful in describing simple nuclear reactions. The theory of multistep direct reactions extends and formalizes these qualitative ideas in a way that includes all the essential quantum-mechanical features of the scattering process such as angular momentum transfer and energy conservation at each step, as well as making some simplifying assumptions to obtain a usable theory. These assumptions include the following.

(1) The chaining hypothesis. This assumption, which would seem to be reasonable, simply assumes that all possible multiparticle interactions are not likely, but that the interaction can only "move" from one stage, the nth, say, to the $(n+1)$th stage, or the $(n-1)$th stage. This is equivalent to assuming that such a transition is induced by the two-body residual interaction. The stages are seen as a particular partition of the Hilbert space and are (usually) interpreted in terms of an increasingly complex m-particle–$(m-1)$-hole type, as in the semiclassical exciton model.

(2) The relative phases of transition matrix elements are assumed to be random, except, in the multistep direct processes, for those that involve the same change in momentum of the particle in the continuum. Thus, the cross sections for a specific step corresponding to a definite angular momentum and energy transfer contribute coherently, but the sum of the contributions from various transitions from one stage to the next is taken incoherently.

(3) The higher the stage, the more "complex" the state and the more accurate the statistical assumptions become. The system is therefore highly likely to move to more complicated states due to the increase in the density of states, and we assume that this is always the case; this is the never-come-back assumption.

These assumptions can be used to derive a formula for the average double differential cross section:

$$\frac{d^2\sigma}{dU\,d\Omega_{\text{direct}}}=\frac{d^2\sigma}{dU\,d\Omega_{\text{single step}}}+\frac{d^2\sigma}{dU\,d\Omega_{\text{multistep}}}\ , \tag{1}$$

where U denotes the excitation energy of the residual nucleus.

The statistical multistep contribution to the cross section was calculated using the expression

$$\frac{d^2\sigma}{dU\,d\Omega_{\text{multistep}}}=\sum_{n=2}\sum_{m=n-1}^{n+1}\int\frac{d\mathbf{k}_1}{(2\pi)^3}\cdots\int\frac{d\mathbf{k}_n}{(2\pi)^3}\left[\frac{d^2W_{m,n}(\mathbf{k}_f,\mathbf{k}_n)}{dU_f d\Omega_f}\right]\left[\frac{d^2W_{n,n-1}(\mathbf{k}_n,\mathbf{k}_{n-1})}{dU_n d\Omega_n}\right]$$
$$\times\cdots\left[\frac{d^2W_{2,1}(\mathbf{k}_2,\mathbf{k}_1)}{dU_2 d\Omega_2}\right]\frac{d^2\sigma_{1i}(\mathbf{k}_1,\mathbf{k}_i)}{dU_1 d\Omega_1}\ . \tag{2}$$

$\mathbf{k}_i$, $\mathbf{k}_n$, and $\mathbf{k}_f$ denote the momenta of the initial-, nth intermediate-, and final-step nucleon, respectively. The exit mode is labeled by m.

The formula shows that the multistep direct contribution is a folding of single-step interactions. The first-step contribution to the overall double differential cross section is given by

$$\frac{d^2\sigma_{1i}}{dU_1 d\Omega_1}=\sum_L (2L+1)R_2(L)\rho_2(U)\left\langle\frac{d\sigma_L^{(\mathrm{DW})}}{d\Omega}\right\rangle . \quad (3)$$

$R_2(L)$ is the spin distribution function, given generally by

$$R_N(L)=\frac{2L+1}{\pi^{1/2}N^{3/2}\sigma^3}\exp\left[-\frac{L(+1/2)^2}{N\sigma^2}\right] , \quad (4)$$

where σ is the spin cutoff parameter, $\rho_2(U)$ is the energy-dependent part of the level density of 1p-1h states in the nucleus after the first collision of the incident particle, and $N=p+h$, the number of particles plus holes.

The transition probabilities from the $(n-1)$th to the nth stage are calculated with distorted-wave Born approximation (DWBA) matrix elements, viz.,

$$\frac{d^2W_{n,n-1}}{dU_n d\Omega_n}=2\pi^2\rho_c(\mathbf{k}_n)\rho_n(U_n)|v_{n,n-1}(\mathbf{k}_n,\mathbf{k}_{n-1})|^2 , \quad (5)$$

where

$$v_{a,b}(\mathbf{k}_a,\mathbf{k}_b)=\int \chi_a^{(-)*}(\mathbf{r}_a)\langle\Psi_f|V(\mathbf{r}_a,\mathbf{r}_b)|\Psi_i\rangle\chi_b^{(+)}(\mathbf{r}_b)d\mathbf{r}_a d\mathbf{r}_b . \quad (6)$$

The MSD contribution proceeds exclusively through states with at least one nucleon being unbound. The density of states of the particle in the continuum is $\rho_c(\mathbf{k}_n)$ for momentum $\mathbf{k}_n$, and $\rho_n(U_n)$ is the density of p-particle, h-hole configurations in the residual nucleus in the nth stage evaluated at the energy U_n. The distorted waves χ are generated from an optical-model potential (e.g., Ref. [12]), and the matrix element connects a nuclear state $n-1$ to a state n via the effective N-N interaction $V_{n,n-1}$. A finite-range Yukawa potential is used for $V_{n,n-1}$, of which the strength V_0 must be adjusted to reproduce the data. The level densities ρ_n are generally calculated in terms of some independent-particle model, such as the equidistant Fermi gas model with Pauli corrections, in which case they are given by the well-known Ericson formula [13]

$$\rho_n(U_n)=\frac{g(gU_n)^{N-1}}{p!h!(N-1)!} , \quad (7)$$

where g, the density of single-particle states in the equal-spacing model, is proportional to the level density parameter a [See Eq. (8), Sec. III B]. A level density parameter a proportional to the mass number A of the target nucleus is usually assumed. In the multistep calculations, a value must also be chosen for the spin cutoff parameter σ.

There has recently been much discussion concerning the correct formulation of the FKK multistep direct theory, in particular whether normal or non-normal DWBA matrix elements of the forms $\langle\chi^-|V|\chi^+\rangle$ or $\langle\hat{\chi}^+|V|\chi^+\rangle$, respectively, should be used [14–16]. The latter are given in the original FKK paper [3], but later Feshbach [16] argued that proper treatment of the statistical averaging converts them to the normal form, in line with numerical calculations [13]. This aspect has been clarified in detail by Feshbach at a recent workshop on multistep direct reactions [17].

B. Calculational details

In the program of Bonetti and Chiesa [18], an important simplifying assumption is made, viz., that the differential transition probabilities in Eq. (5) do not depend on the stage of the chain. The density $\rho_n(U_n)$ describes the final states of the interaction when a particle in the continuum collides with a bound nucleon and creates a particle-hole pair. The final-state density is therefore assumed to be that of the particle-hole pairs, that is, $\rho_n(U_n)=\rho_2(U_2)$ for all n. Using the Ericson expression for the level density with $N=2$ gives a differential cross section proportional to $(g^2)^n$, and therefore also to $(a^2)^n$ if there are n stages in the multistep chain. Since the effective interaction enters at each stage of the reaction, the final n-stage cross section is also proportional to $(aV_0)^{2n}$—hence the level density parameter and the effective interaction strength have to be considered simultaneously when parameters of the calculations are fixed *a priori*.

The main physical input for the program of Bonetti and Chiesa relates to the DWBA calculations performed with the code DWUCK4 [19]. These include the following.

(1) Optical-model parameters. In the present case these were taken from the universal parameter set of Schwandt *et al.* [12]. In order to evaluate their effect on the results, the optical potentials due to Madland [20] were also used—see Sec. IV C 1 below.

(2) The effective interaction. Here we use a Yukawa interaction with a range of 1 fm. There has been a great deal of theoretical work done on effective interactions in the last 20 years, but we have kept this empirical interaction for a number of reasons. Mainly, it allows us to make a comparison with other work using this approach. A significant reduction in the strength of the effective interaction has been seen at energies above 100 MeV [6,7]. The results of this article confirm this and greatly extend the analyzed data in this region. Detailed studies of the effective interactions, based on G matrices extracted from the shell model or from fitted N-N interactions such as the Paris potential, have considered the various terms of the interaction, V_{ST}, where S and T, the spin and isospin transferred in the interaction, may have the values 0 and 1. In our (p,p') data all these terms occur for the central part of the interaction, and for the noncentral parts those with $S=1$. Because of uncertainties in the relative magnitudes of the various terms, it is simpler to employ a central empirical interaction of which the strength is fitted to best reproduce the data. Our approach has thus been to use the Yukawa interaction of range 1 fm and vary its strength to obtain the best overall normalization.

As will be shown, the resulting strengths show a definite reduction as a function of incident energy if we use an overall V_0 for each incident energy. The effect of making it energy dependent for the multistep parts is investigated in Sec. IV C 4.

(3) The choice of particle-hole configurations. The selection of the combinations of particle-hole states used to obtain the form factors, which correspond to different energy transfers (E) and angular momentum transfers (L), is done as follows: The spherical Nilsson shell model is used as a guide to which levels will give the desired E and L transfers. For ease of calculation, the E transfers are divided into "bins" of roughly 20 MeV. For each L and E bin, a suitable p-h set is then chosen. The specific chosen levels only serve as a model for the transition. Clearly the "single-particle" levels in real nuclei are spread over many levels even at low excitation energy. The single-particle wave functions used in the form factor calculation are obtained by adjusting the depth of a standard Woods-Saxon well to obtain the desired energy transfer. The one level is chosen at an energy equal to the negative of the separation energy of the excited nucleon and the other lower by an amount equal to the required change in energy of the particle in the continuum. Thus, the form factor is sensitive to the change in energy between the two levels.

Several problems arise in this procedure. The well depths for the different calculations which make up a specific E transfer for various L-transfer values can differ substantially. This is probably not too serious, since each calculated cross section simply serves as a model for that transfer. Since mainly the low L-transfer values contribute to the overall cross section, several combinations are chosen for these transfers, and the average taken. The maximum number of values of the angular momentum transferred in the reactions varied between 7 and 9, with the largest value used for the highest incident energies (175 and 200 MeV).

Further problems arise in choosing the levels for a specific energy and L transfer where no p-h combination exists in the simple shell model: (a) For lower-energy transfers, we have "borrowed" a combination from the next lower-energy bin. The search routine will then fix these at energies which correspond to the required E transfer. This seems to be a reasonable procedure, since the lack of a level is probably due to the simplicity of the model used. (b) For large energy transfers, the above procedure sometimes leads to an unrealistically high excitation energy for a single-step process, and would lead to another unbound particle since the well depth is limited. Since the depth of the potential for the lowest levels in the nucleus is not precisely known (the possible levels around the Fermi level are not very well defined either), it is not certain when such excitations should be terminated.

This problem was not serious in most earlier studies since the possible energy transfers were limited by the entrance channel energy. In this paper we have neglected the transitions for which no transfers were found in the cases for incident energies of 150, 175, and 200 MeV.

Another aspect of the choice of particle-hole configurations should be mentioned here. In the first step more than one configuration is used for the important transitions, whereas in the multistep part of the program of Bonetti and Chiesa [18] only one configuration is used for each value of the angular momentum transferred in an energy bin. It would seem that it is also necessary to include more configurations for the multistep part since, at the higher energies, this part is now as important as the first step in many cases.

(4) The level density parameter a. In terms of importance this input parameter is on an equal footing with the strength V_0 of the effective interaction since the cross section is proportional to $(aV_0)^{2n}$ for an n-stage process. An expression for the level density based on the Fermi gas model is generally employed. Such a simple model should be adequate for the purpose of these statistical calculations, but which level density parameter to use is a problem. Values have been measured for most nuclei, but these measurements relate to level densities at very low excitation energies. At low temperature in the independent-particle model, the level density parameter is proportional to the density of single-particle states near the Fermi energy. At zero temperature [21],

$$a=\tfrac{1}{6}\pi^2 g(\epsilon_F)\ . \tag{8}$$

As the excitation energy increases, the shell effects in the level density weaken, and at high enough excitation energies (about 100 MeV) the mass-number dependence of a tends to the simple quasiclassical limit [22] $a=\text{const}\times A$. For this reason we have generally employed $a=A/8.5$ MeV^{-1} in our calculations.

Another aspect of the level density parameter is its explicit dependence on the excitation energy. Several theoretical approaches to this question exist in the literature [22–24]. In Sec. IV C 3, the results obtained with a simple energy-dependent a are presented.

(5) The spin cutoff parameter σ in the single-particle level density. In the multistep calculations a value must

TABLE I. Values of the strength of the effective interaction V_0 obtained from the present work (based on a Yukawa potential of range 1 fm).

Target	E_p (MeV)	V_0 (MeV)	a	σ
^{58}Ni	100	23.8	6.82	2.5
	120	23.0	6.82	2.5
	150	21.0	6.82	2.5
	175	20.5	6.82	2.5
	200	18.0	6.82	2.5
^{100}Mo	100	22.0	11.8	2.5
	120	16.7	11.8	2.5
	150	14.0	11.8	2.5
	175	13.5	11.8	2.5
	200	12.5	11.8	2.5
^{197}Au	100	18.5	23.2	3.5
	120	12.5	23.2	3.5
	150	11.5	23.2	3.5
	175	10.3	23.2	3.5
	200	9.4	23.2	3.5

also be chosen for the spin cutoff parameter σ. A variety of values of σ were tried for each target and incident energy, and those that gave the best overall agreement were used in the final calculations. These values of σ, together with values of V_0 and a used for our calculations, are given in Table I. A value of 2.5 was found appropriate for both ^{58}Ni and ^{100}Mo, but for ^{197}Au a higher value, viz., 3.5, gave significantly better results. The effect of σ was relatively more important at higher incident energies.

After setting $a = A/8.5$ MeV^{-1} as described above, the calculated cross sections were normalized by choosing values of V_0 to give the best overall agreement with experiment. Finally, it should be mentioned that the number of partial waves L_{max} used in the DWBA calculations varied between 30 and 70, and the number of steps employed in the calculations varied from 5 for the lower to 6 for the higher incident energies.

IV. RESULTS AND DISCUSSION

A. Comparison of theoretical and experimental angular distributions

The angular distributions for the targets ^{58}Ni, ^{100}Mo, and ^{197}Au at various incident energies are given in Figs. 1–3 and 4(a)–(c) for a range of energies of the emitted proton (or equivalently, excitation energy of the residual nucleus $U = E_p - E_{p'}$ if it is assumed that only one particle is emitted).

For an incident proton energy of 100 MeV, the FKK calculations provide a good description of the experimental data (at the higher excitation energies in particular) for all three targets. For lower excitation the theory generally falls below the experimental points—however, in this region collective effects may be expected to contribute significantly to the cross section. The quality of the agreement between experiment and theory is similar for the Ni and Mo targets, while the shape of the angular distribution is somewhat less satisfactory for Au—normalizing to produce agreement at forward angles results in the calculated distribution being too low at large angles, and vice versa.

For 120-MeV incident energy, excellent agreement is found for the Ni and Mo targets at the higher excitation energies. The agreement gets progressively worse as the excitation energy decreases and eventually the MSD calculations fail to produce the correct shape. For Au the overall agreement is good, but the calculated shape of the angular distribution is less satisfactory at the highest excitation energy.

The agreement between experiment and theory for 150-MeV incident energy for the three targets is similar to that for 120 MeV, although the results for Au now appear to be better at the higher excitation energies. At 175-MeV incident energy [Figs. 4(a)–4(c), solid lines], the calculated angular distributions for all three targets are reasonable—some deviations occur at the lowest emission energy (60 MeV) as well as at the two highest emission energies, and at larger emission angles.

For 200-MeV incident energy, the general agreement is good, except again at the largest and smallest emission energies. For the Ni target, the results are not as good as for Mo and Au, although the overall results at the other incident energies have been superior for Ni. A noticeable feature for all three targets at this incident energy is that the theory once again underestimates the cross section at the highest and lowest excitation energies.

On the whole, the MSD calculations reproduce the angular distributions for the three targets quite well—some discrepancies between experiment and theory are evident at low excitation energies irrespective of the incident energy, and at high excitation energies for the higher incident energies (175 and 200 MeV) in particular. This may be due to a variety of factors, such as contributions from secondary processes or deficiencies in the global optical potential used at these energies [12]. It is significant that, for the lower incident energies, the general agreement extends over more than 3 orders of magnitude for the highest emission energies.

Part of the discrepancy between theory and experiment may be due to transitions from the P to the Q chain after the first step, which can give multistep compound contributions to the cross section even at high incident energies where the feeding of the Q chain from the entrance chan-

TABLE II. Values of the strength of the effective interaction V_0 obtained from previous work (also based on a Yukawa potential of range 1 fm).

Reference	Reaction	V_0 (MeV)
Austin, 1980[a]	(N,N') discrete states, 20–50 MeV	27.9
Holler *et al.*, 1985[b]	(p,n) 26.7 MeV MSC+MSD	27
Mordhorst *et al.*, 1986[c]	(p,n) 25.6 MeV MSC+MSD	25
Marcinkowski *et al.*, 1989[d]	(n,n') 11.5, 26 MeV MSC+MSD	25
Trabandt *et al.*, 1989[e]	(p,n) 80 MeV MSD	20±1
Scobel *et al.*, 1990[f]	(p,n) 120 MeV MSD	16±1
Cowley *et al.*, 1991[g]	(p,n) 160 MeV MSD	12.5±1
	(p,p') 80 MeV MSD	23
	(p,p') 120 MeV MSD	17.5

[a]Reference [27].
[b]Reference [28].
[c]Reference [29].
[d]Reference [30].
[e]Reference [6].
[f]Reference [7].
[g]Reference [8].

nel is negligible. Studies at lower incident energies have shown that the total statistical contribution to the cross section is somewhat greater than would be expected from the entrance channel width, suggesting the presence of later P to Q chain transitions [25,26]. Such transitions could give appreciable multistep compound contributions to the cross section even at high energies where the entrance channel width has become very small.

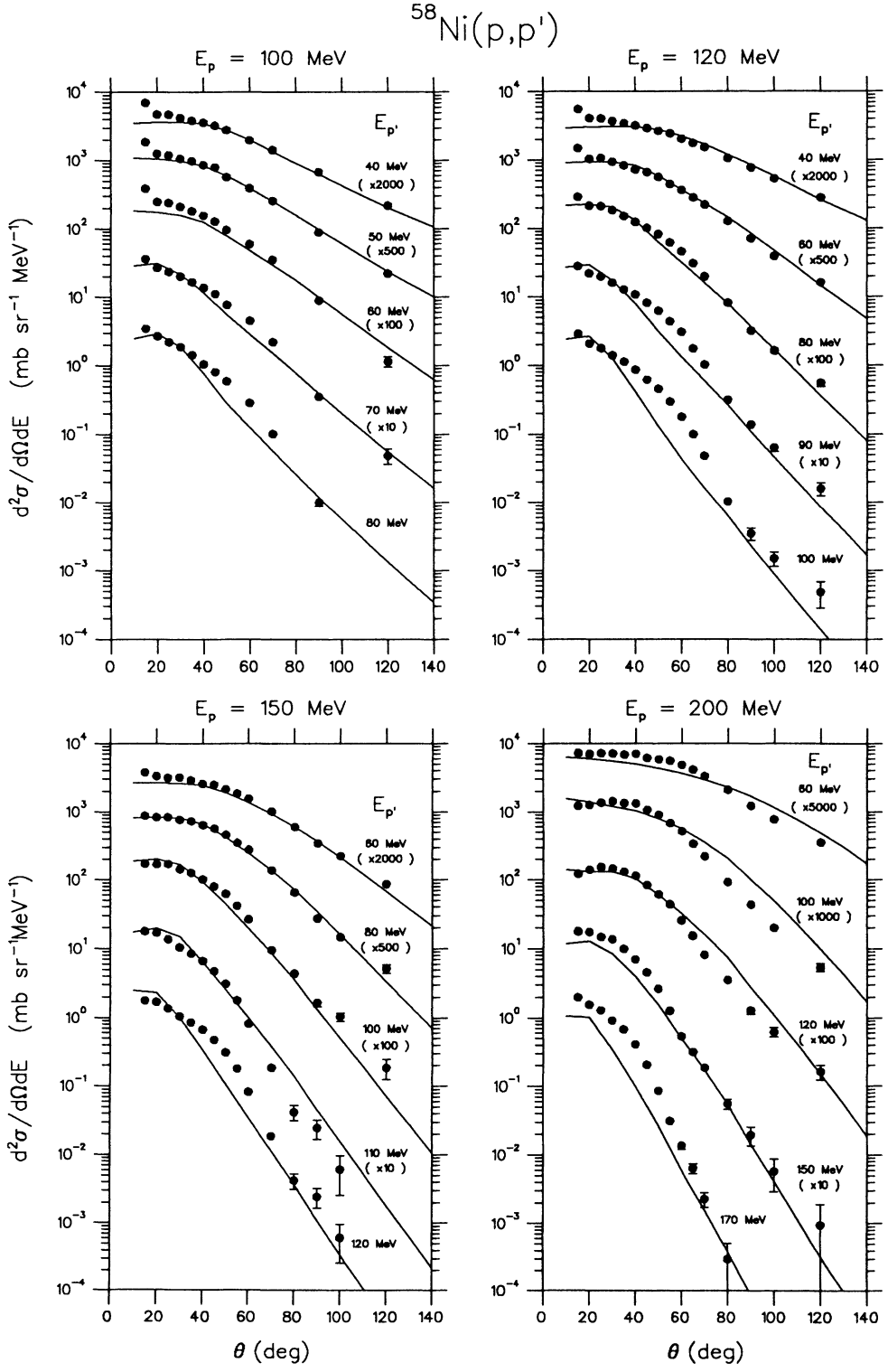

FIG. 1. Experimental angular distributions for ^{58}N(p,p') at various incident energies E_p and emission energies $E_{p'}$. Statistical error bars are shown where these exceed the symbol size. The curves are results of MSD calculations. Results are multiplied by the indicated factors for display and are given in the laboratory system.

B. The effective interaction V_0

It is of interest to compare our V_0 values (Table I) with the results of several analyses as listed in Table II. Some of these are compared with the present results for ^{100}Mo(p,p') in Fig. 5. These calculations all used harmonic-oscillator wave functions for the bound nucleons, optical-model wave functions for the emitted nucleons, and Yukawa two-body interactions with a range of 1 fm. The spread in values of V_0 is due partly to the

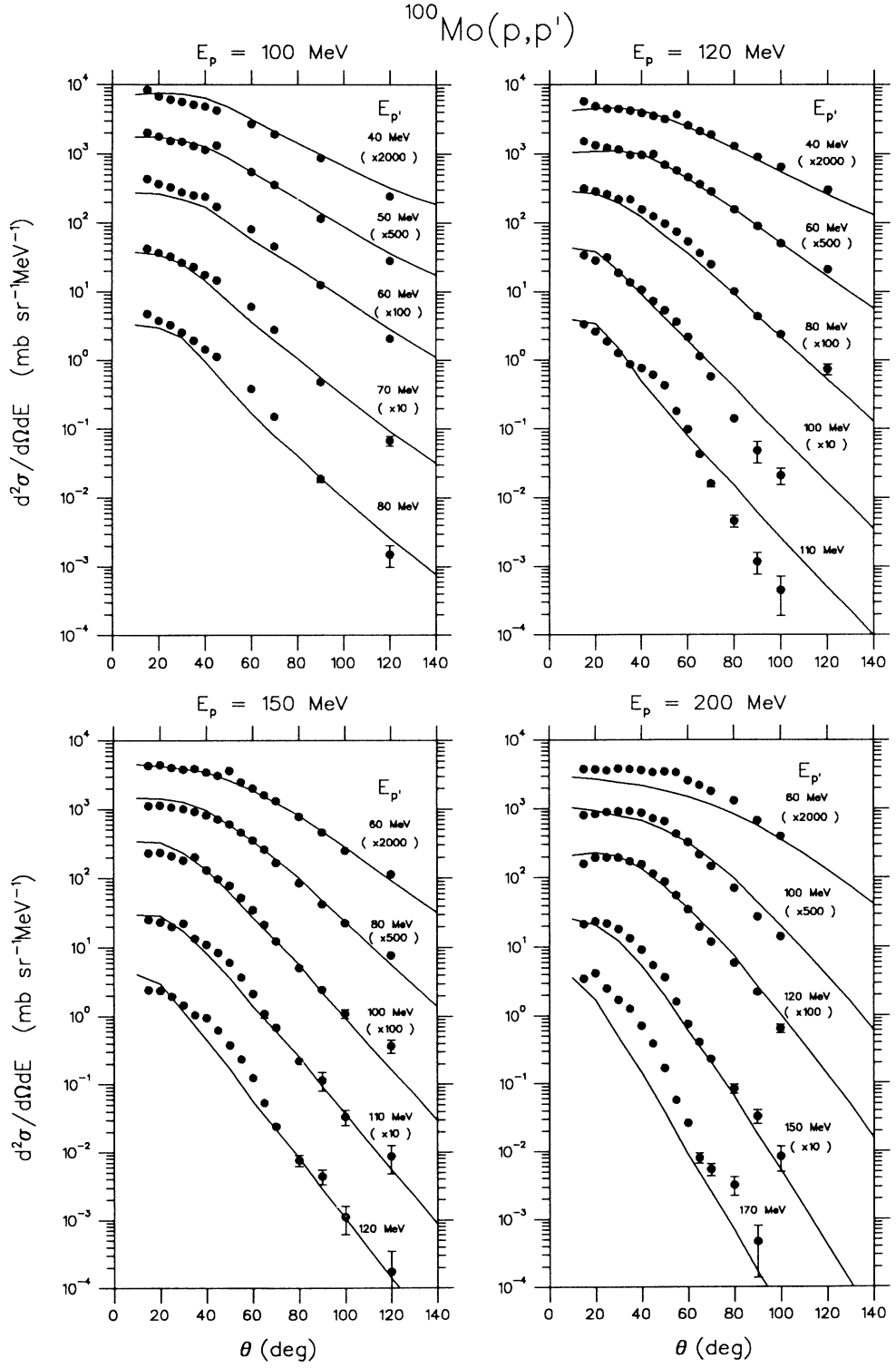

FIG. 2. Experimental angular distributions and MSD calculations for ^{100}Mo(p,p'). See also caption to Fig. 1.

differences in the analyses and also the energy dependence of the effective interaction. Some analyses were made which distinguish between neutrons and protons in the cascade of intranuclear steps; this had a rather small effect (less than 10%) on the shape of the cross section, but required an increase of V_0 in the case of recent analyses of (p,n) reactions [31].

The values of V_0 are found to decrease monotonically with increasing incident energy, and this is indeed what would be expected from the related decrease of the real

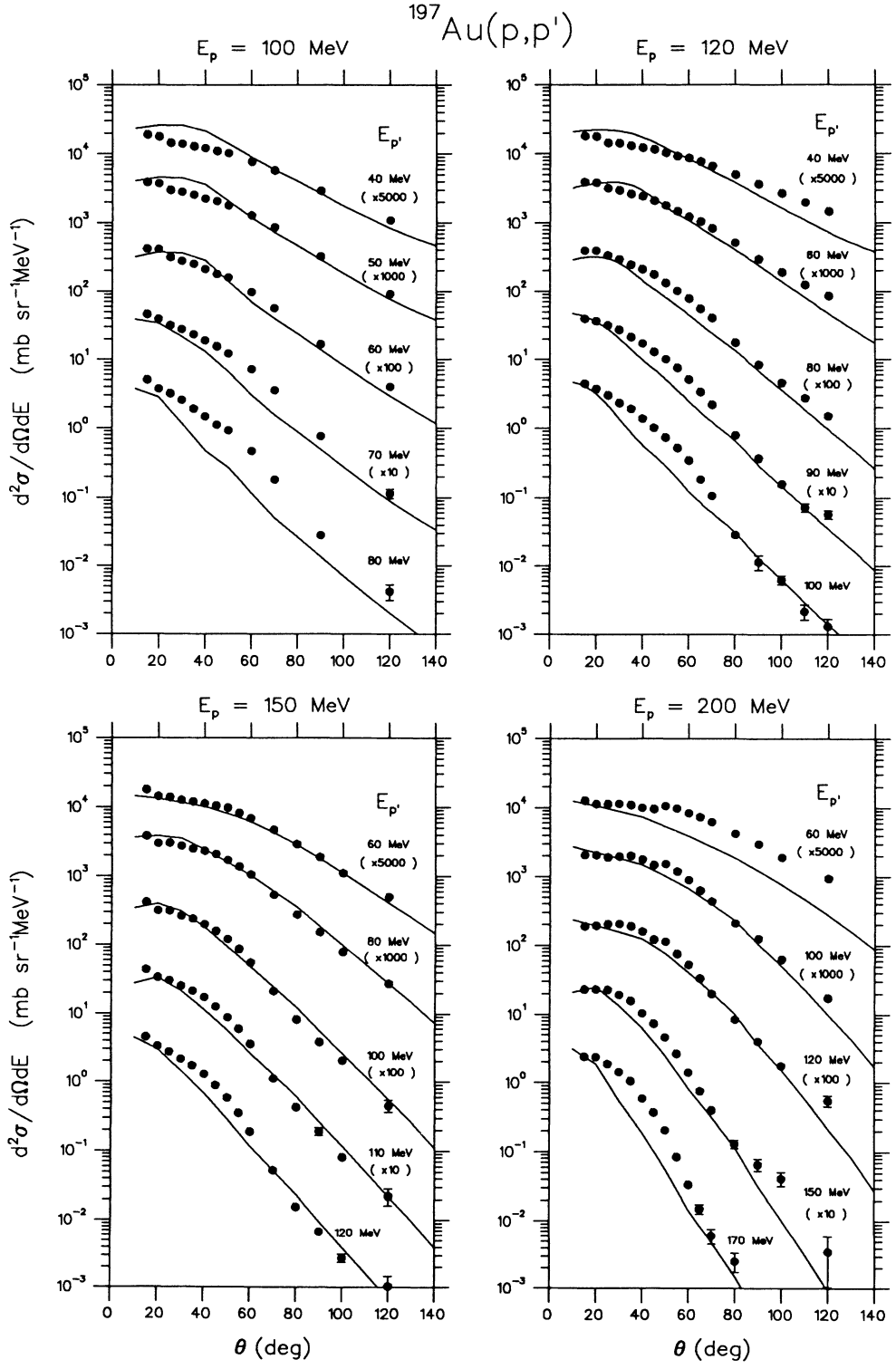

FIG. 3. Experimental angular distributions and MSD calculations for ^{197}Au(p,p'). See also caption to Fig. 1.

optical potential, which also depends on the strength of the effective two-body interaction. The curve $V_0 = 30.8 \exp(-0.15E/30.8)$ in Fig. 5 is obtained from the energy dependence of the optical-model potential as described in Ref. [8].

The differences in V_0 for the various target nuclei require comment (see Fig. 6). The result for Mo seems to correspond quite well with values found earlier. All V_0 values appear to have a similar energy dependence as well, but the values for Ni seem too high and those for

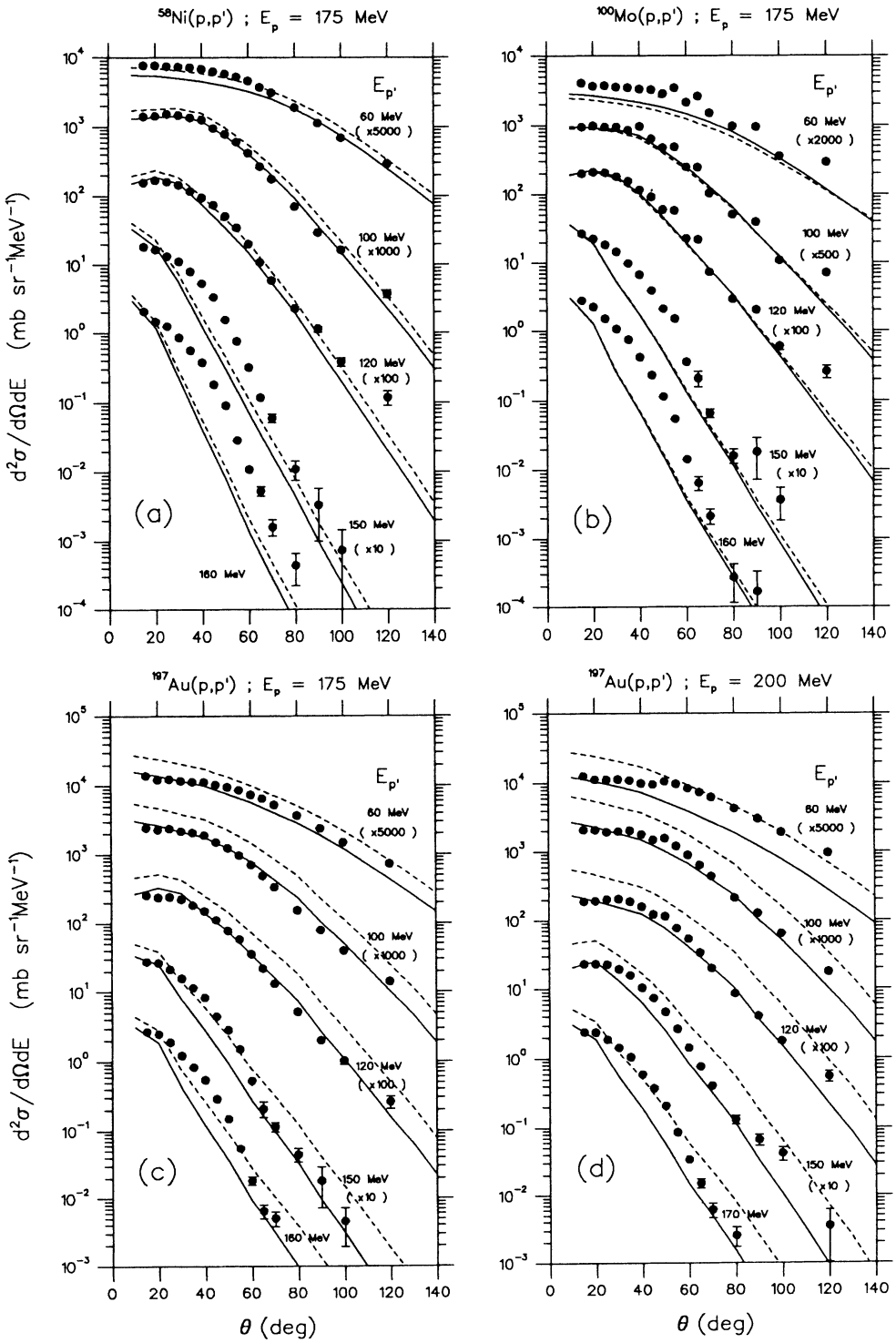

FIG. 4. The sensitivity of MSD calculations to changes in the optical potentials. The solid curves are obtained with the global potential of Schwandt *et al.* [12]. The dashed curves in (a), (c), and (d) are for calculations with the Madland potential [20] and in (b) for an arbitrary increase of 10% in the depth of the real potential. See also caption to Fig. 1.

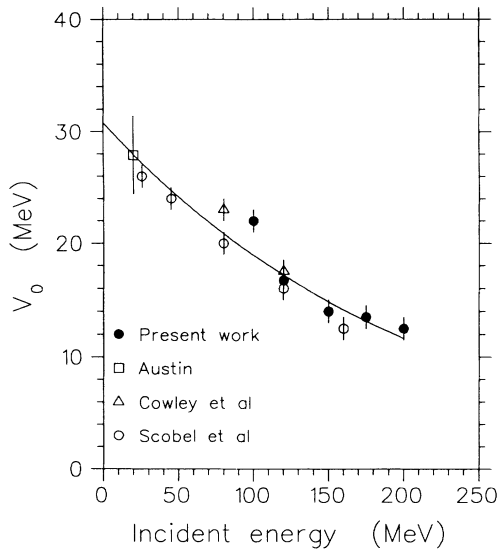

FIG. 5. The effective interaction strength V_0 as a function of incident energy. The values obtained in this work for the ^{100}Mo(p,p') reaction are compared with values given by Scobel *et al.* [7], Cowley *et al.* [8], and Austin [27]. The solid curve indicates the normalized energy dependence of the optical potential, as discussed in the text.

Au too low. Possible reasons for this result include the following.

(1) The level densities may not follow the trend of $A/8.5$. The formula in Ref. [22] has an A^2 dependence which would increase (reduce) the value of the level density for Ni (Au) relative to that of Mo, implying a decrease (increase) in V_0 by the same amount. Although this behavior is in qualitative agreement with the trend in Fig. 6, the predicted differences are considerably smaller than those observed (see also Sec. IV C 3 below).

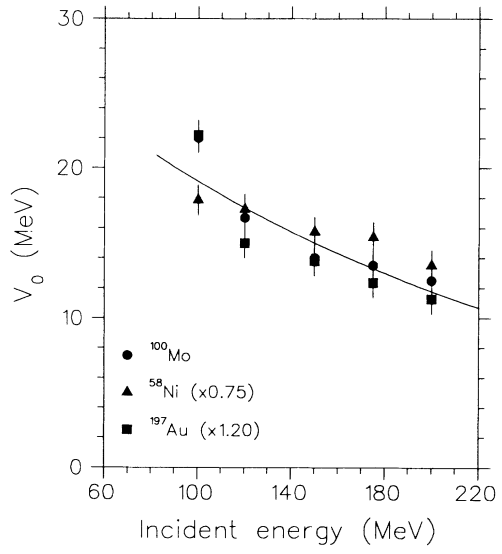

FIG. 6. The effective interaction strength V_0 as a function of incident energy for different target nuclei. The results for ^{58}Ni and ^{197}Au have been arbitrarily normalized by the indicated factors. The solid curve is as in Fig. 5.

(2) The various components of the effective interaction may act differently in the first-step excitation of these nuclei, as the isospin structure, for example, of the targets could be different.

(3) The Schwandt optical-model potential has an A dependence and may cause a systematic difference depending on the target nucleus.

(4) The exact p-h combinations chosen for the various steps should not play a major role in the final result due to the extensive summation and averaging that occurs, but this may have an effect. This is unlikely though, since the configurations were selected anew for each incident energy, and the V_0 values are consistently lower for Au compared to Ni.

C. Investigation of possible sources of disagreement

1. Sensitivity to optical-model potentials

Our calculations of the incoming and outgoing distorted waves were based on the global optical-model potential of Schwandt *et al.* [12]. This potential was obtained from fits to proton elastic-scattering cross sections and analyzing powers for nuclei in the mass range $24 < A < 208$, with incident proton energies between 80 and 180 MeV. To assess the effect of using a different potential, we have repeated some of the calculations with the Madland [20] global optical-model parameters, which are expected to be valid over a larger energy range ($50 \leq E_p \leq 400$ MeV). The starting point for this work was the Schwandt potential, and only the absorptive part of the central potential was modified to reproduce the reaction cross sections for the three nuclei ^{27}Al, ^{56}Fe, and ^{208}Pb. In Fig. 4(a), for a ^{58}Ni target with incident proton energy of 175 MeV, it can be seen that the Madland global optical potential produces a slightly larger cross section for the same value of the effective interaction V_0, but the general shape is very similar to that of the Schwandt potential. The effect of using the Madland potential is therefore to introduce a renormalization of the effective interaction strength V_0, in the present case lowering the value of V_0 from 20.5 to 19.2 MeV. A further illustration of the sensitivity of the optical potential is provided in Fig. 4(b) for ^{100}Mo at 175-MeV incident energy, in which the depth of the real optical potential V_R was increased arbitrarily by 10% and the radius parameter r_R decreased to retain the same value of $V_R r_R^2$.

In Figs. 4(c) and 4(d), similar comparisons between results of the Schwandt and Madland potentials are shown for a ^{197}Au target at 175- and 200-MeV incident energy. Once again the shape is very similar with the Madland optical potential, but the effect on the effective interaction V_0 is more dramatic, which will then require a larger relative reduction in V_0 (from 10.3 to 9.4 at 175 MeV and from 9.4 to 8.3 MeV for 200 MeV). These results emphasize the importance of the choice of the optical-model parameters on the value of the effective interaction extracted from the data, and indicate that caution should be

used in comparing values of V_0 obtained from different potentials at higher incident energies.

2. *Multiparticle emission*

In order to investigate multiparticle emission in general, and specifically its relationship to the steeper falloff in the angular distributions at higher incident energy, we have attempted a simulation based on quasifree knockout for ^{58}Ni. While the procedure of adding this component incoherently to the MSD cross sections should be only considered to be a very crude approximation to a proper microscopic inclusion of such a contribution, it nevertheless serves to illustrate the qualitative expectation.

A pure quasifree nucleon knockout component was calculated in the distorted-wave impulse approximation (DWIA) as in Ref. [11], except that distorted waves were used for both emerging nucleons, instead of one. As implied by the results discussed in Ref. [11], this amounts to requiring that two nucleons emerge as free nucleons after a quasifree collision.

The sum of the MSD and DWIA cross sections, with spectroscopic factors as required in Ref. [11], and also with the DWIA results arbitrarily doubled, is shown in Fig. 7. The inclusion of two-nucleon emission is demonstrated to improve the agreement at low excitation (i.e., high emission) energy where the multistep contribution is suppressed, whereas the results at high excitation are altered relatively little. It was also found that, at 100- and 120-MeV incident energy, the good agreement between the MSD and experimental cross sections is retained due to the fact that the knockout component is somewhat suppressed.

3. *Energy dependence of the level density parameter*

The phenomenological relation developed in Ref. [22] can be used to consider the effects of the energy dependence of the level density parameter. The energy dependence of a can be expressed as a function of the excitation energy U and the "shell correction factor" δW (the difference in mass of the nucleus and the value predicted by the liquid-drop model) as $a(u)=\tilde{a}[1-f(U)\delta W/U]$, where the asymptotic value of the density parameter at high excitation energy is given by $\tilde{a}=\alpha A+\beta A^2$, and $f(U)=1-\exp(-\gamma U)$. The coefficients α and β are listed in Ref. [22]. Figure 8 shows the effect of renormalizing the various DWBA cross sections according to this prescription for proton scattering from ^{58}Ni at 200 MeV. The V_0 value has been rescaled to give the average normalization correctly. The resulting distributions are not very different, but the cross sections for highly excited states are pushed up relative to that for the lower excitation exit channels. This is to be expected since the excitation energy dependence of the level density parameter will reduce the importance of the first step which dominates the low excitation cases.

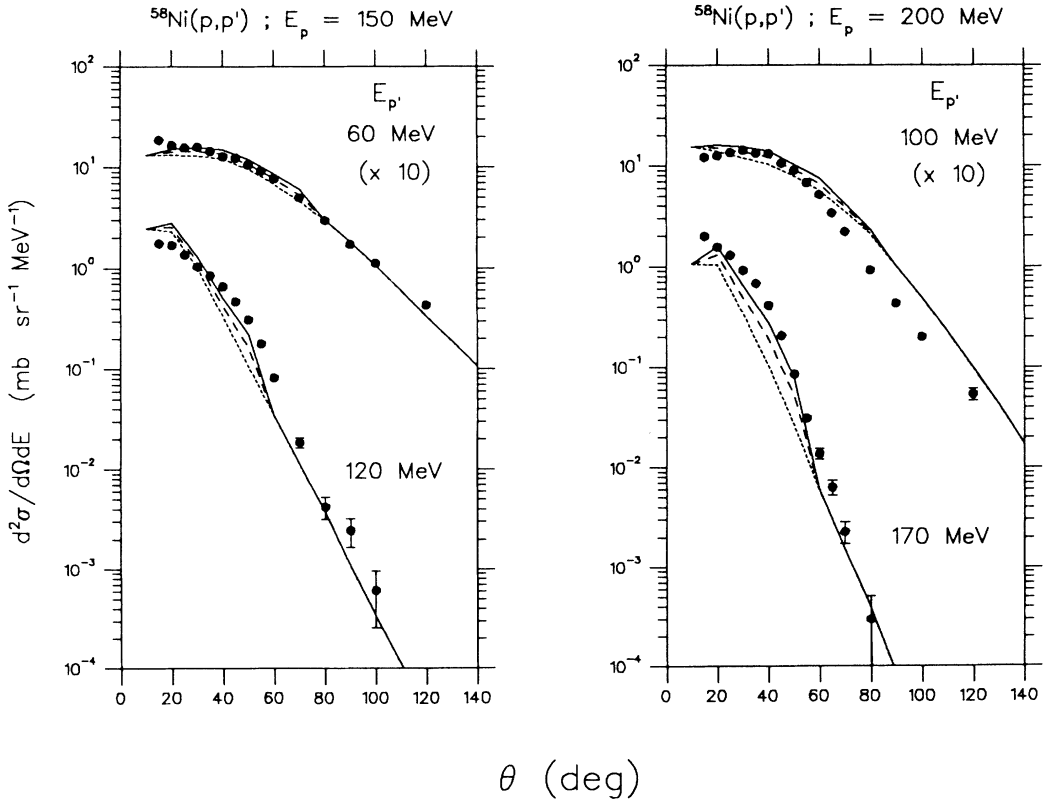

FIG. 7. The effect of multiparticle emission on MSD calculations. The curves correspond to MSD only (dotted line), MSD plus quasifree knockout (dashed line) and MSD plus twice the quasifree-knockout component (solid line).

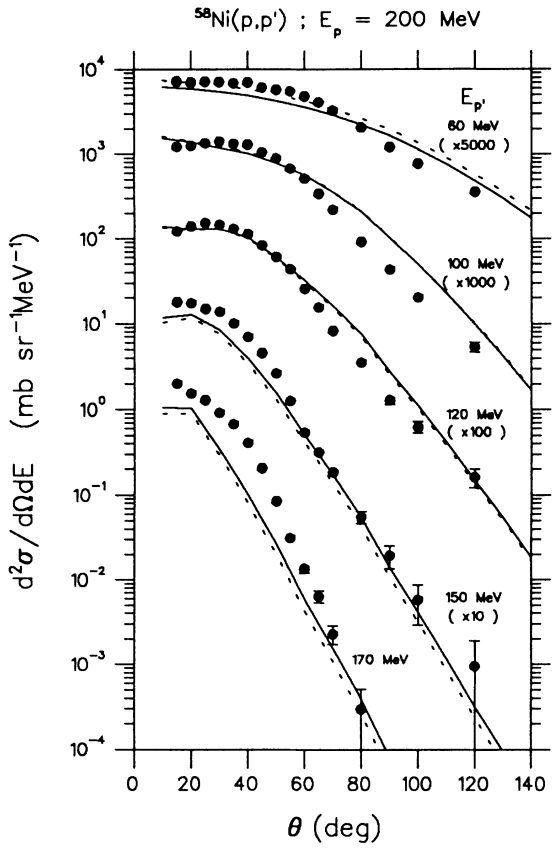

FIG. 8. The effect of the energy dependence of the level density parameter on MSD calculations. The dashed curve is obtained with an energy-dependent level density parameter and the solid curve is obtained with a constant value.

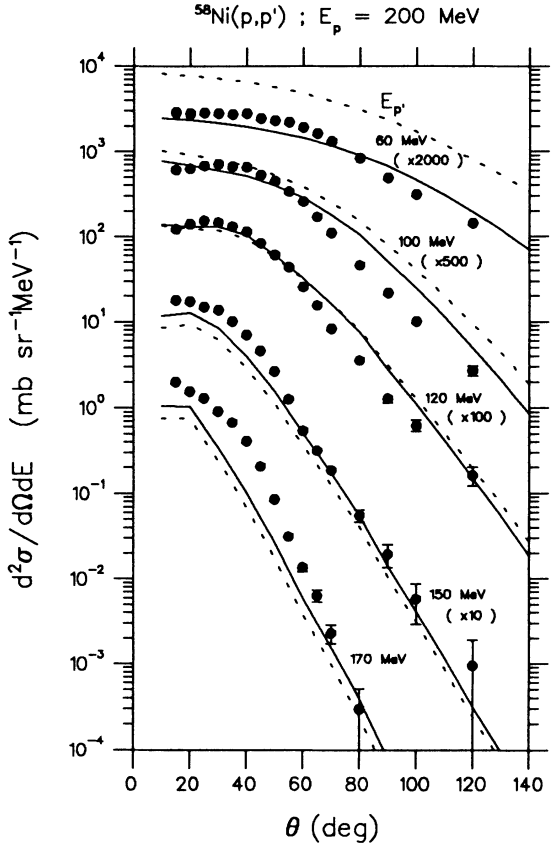

FIG. 9. The effect of the incident-energy dependence of the effect interaction V_0. The solid curves are MSD calculations with a constant V_0 for all steps while the dashed curves are obtained when the energy dependence of V_0 is taken into account in the multistep part of the calculation.

4. Step variation of V_0

The incident-energy dependence of V_0 leads to a slight inconsistency in the calculational procedure. In the multistep part of the calculation, we are performing DWBA calculations at lower incident energies. Thus, V_0 should be different for each stage. To gauge the importance of this effect, we have renormalized the cross sections for the different stages according to a V_0 dependence given by the experimental curve in Fig. 4, which can be approximated by an exponential function (see Ref. [8] and Sec. IV B). This leads to a bigger emphasis on the higher steps since they take place at "lower" incident energy where the effective interaction is larger. Figure 9 illustrates the importance of this effect—it is not very significant except for very high excitation energies.

D. Emission-energy dependence of contributions from various steps

The contributions of the various MSD steps to the angular distributions for different emission energies are shown in Fig. 10 for an incident energy 150 MeV for ^{58}Ni. Also shown in Fig. 10 are the relative contributions of each step. Clearly the first step diminishes in importance towards larger angles for all excitations of the residual system shown in Fig. 10, and only for the lowest excitation shown (emission energy of 120 MeV) is the first step dominant for forward scattering. This observed trend is not unexpected.

E. Incident-energy dependence of contributions from various steps

As an example of the incident-energy dependence of the results, decomposed into the various MSD steps, calculations for the target nucleus ^{58}Ni are shown in Fig. 11 at a fixed excitation energy (30 MeV). The cross section for the first step is observed to fall off at an increasingly rapid rate with incident energy as a function of angle.

Similarly, the other steps in the multistep chain have their maximum relative contributions at smaller scattering angle with increasing incident energy. This behavior is consistent with increasing forward peaking with increasing incident energy.

F. Comparison between first-step contributions predicted by MSD and quasifree knockout

As was mentioned by Förtsch *et al.* [11], the correspondence between the first-step component predicted by the MSD theory and that calculated in DWIA (as

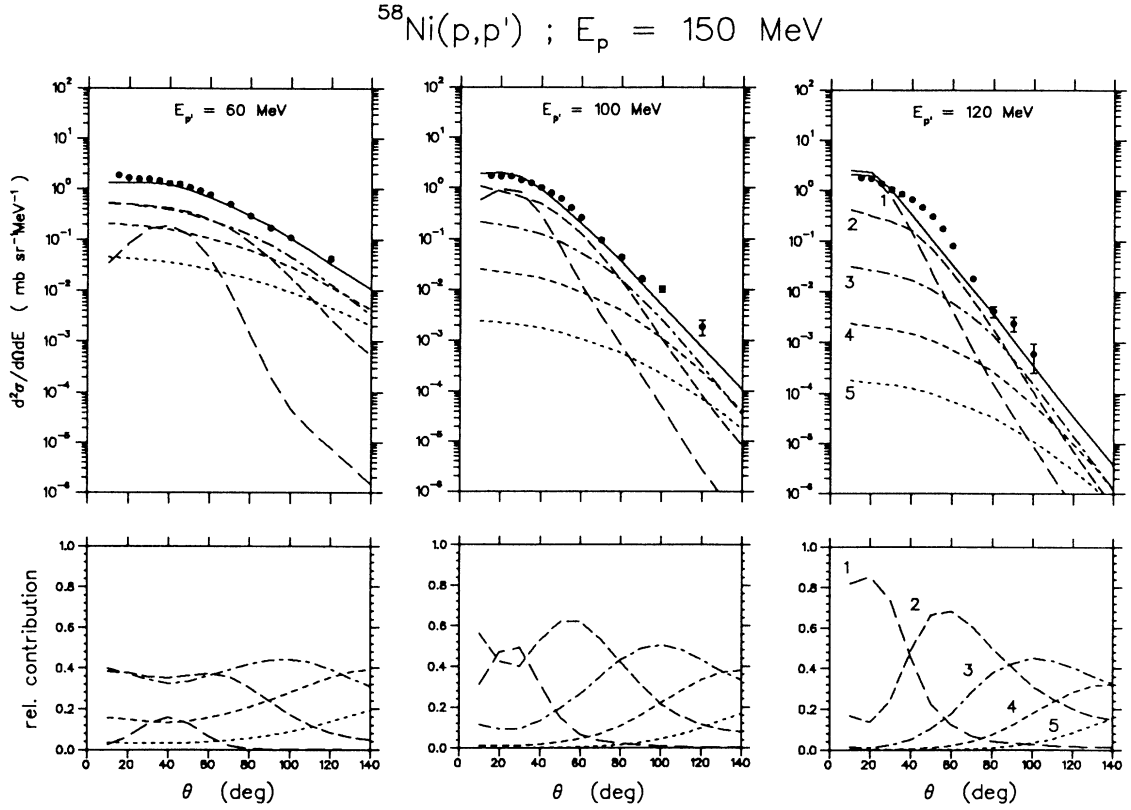

FIG. 10. The emission-energy dependence of the absolute (upper panels) and relative contributions of the leading five MSD steps to the angular distribution for ^{58}Ni(p,p') at an incident energy of 150 MeV. The various dashed curves in the right-hand panels are labeled by the step number. The solid curves are the sums of the indicated step contributions.

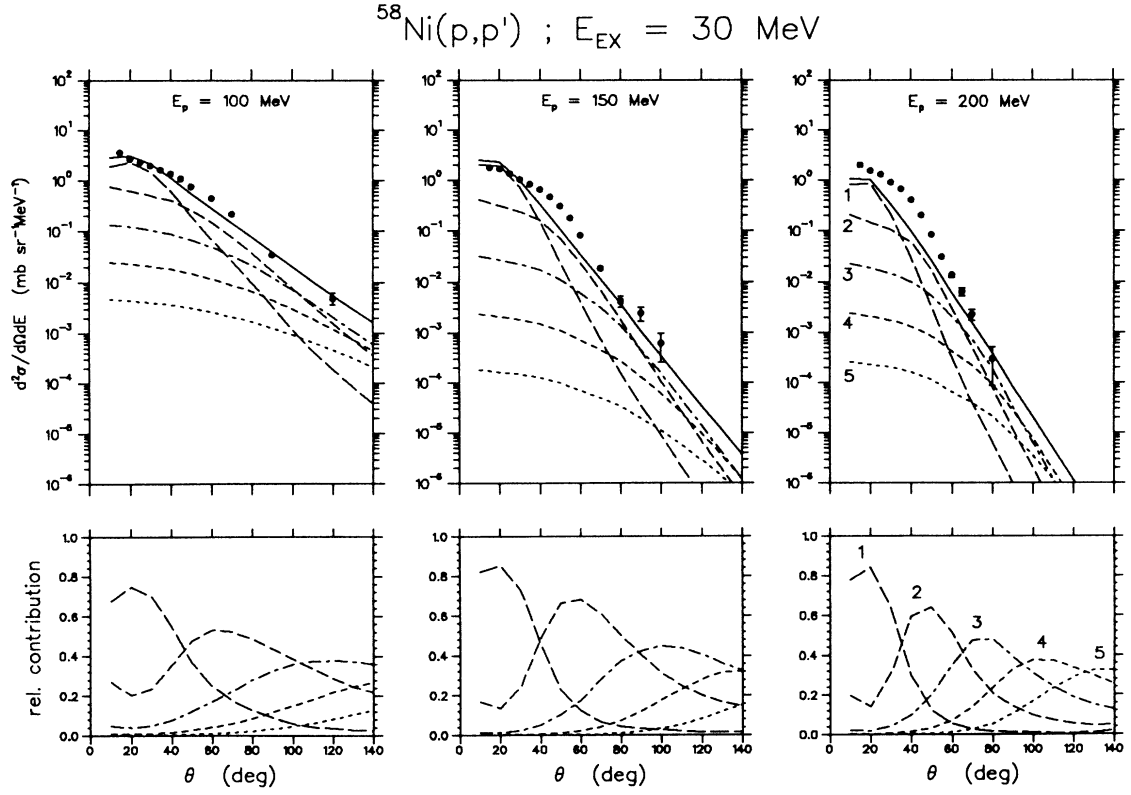

FIG. 11. The incident-energy dependence of absolute and relative contributions of the leading five MSD steps to angular distributions for ^{58}Ni(p,p') at an excitation energy of 30 MeV. See also the caption to Fig. 10.

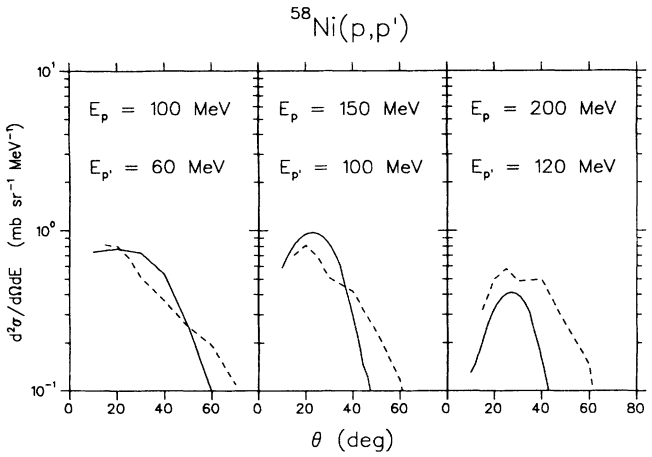

FIG. 12. A comparison between the first-step MSD contribution (solid line) and a quasifree-knockout component calculated in DWIA (dashed line).

described in Ref. [11]) is remarkable. In Fig. 12, results are shown for ^{58}Ni at incident energies of 100, 150, and 200 MeV at $E_{p'} \approx 0.6 E_p$. These comparisons, which cover a larger range of incident energies than that of Ref. [11], show that the two models are in reasonable agreement, even at 200 MeV where the first-step angular distributions are still in good shape agreement. However, at the highest energy, the absolute magnitudes differ somewhat.

It should be pointed out that the DWIA calculations include the two-nucleon emission implicitly, but, as described in Sec. IV C 2, this component is not expected to be significant at the emission energies of Fig. 12. Thus, the quantitative difference in the first step at an incident energy of 200 MeV cannot be ascribed to the effect of two-nucleon emission.

V. SUMMARY AND CONCLUSIONS

It has been shown that the statistical multistep direct theory of Feshbach, Kerman, and Koonin successfully reproduces the (p,p') continuum angular distributions of the three nuclei ^{58}Ni, ^{100}Mo, and ^{197}Au over a range of incident energies from 100 to 200 MeV, and a wide range of proton emission energies, for an angular range between 20° and 120°. For the lowest excitation energies (typically 20–30 MeV), where the theory generally underestimates the cross section, it has also been shown by a DWIA calculation that quasifree nucleon knockout can make a significant contribution. A more complete and accurate calculation of the two-nucleon emission cross section could possibly account for such a discrepancy. Some systematic deviation between theory and experiment has also been found at high excitation energies for the highest incident energies (typically 175 and 200 MeV). In the multistep calculations, various input parameters of the theory have been varied, and increases in the number of steps in the multistep cascade, the number of partial waves used, and the number of angular momenta transferred have not resolved this discrepancy.

The correspondence between theoretical and experimental angular distributions for a particular target shows a reasonably consistent behavior as a function of incident and excitation energy. In general there is a gradual deterioration of the agreement from low to high incident energies, and also towards the lowest and highest excitation energies. The results for the three targets are very similar. For ^{197}Au, a larger value of the spin cutoff parameter σ (3.5) had to be used than for the other two nuclei, for which a value of 2.5 gave good results. The effect of the value adopted for σ appears to be relatively more important at higher incident energies.

The behavior of the strength V_0 of the effective two-body interaction assumed, viz., a simple Yukawa interaction with 1-fm range, as a function of incident energy, is similar for all three nuclei. There is a monotonic decrease as the incident energy increases, and this can be well described on average by an exponential function which follows the energy dependence of the real part of the optical-model potential. This trend is also found in other experiments. However, the values of V_0 for the individual nuclei are systematically different for the same incident energy. We have shown that, when the energy dependence of the level density parameter (which is proportional to the single-particle level density) is taken into account, a mass dependence follows—however, the magnitude is not sufficient to explain the noted differences, and further study into this effect will be required.

The effect of taking into account the explicit energy dependence of V_0 (from the average exponential curve described above) for the successive steps in the multistep chain, rather than using an overall single strength, has also been investigated. This amounts to using progressively larger values of V_0 for the later steps associated with lower incident energies in the DWBA calculations. It is concluded that the effect is rather small.

The sensitivity of the calculations to different optical-model potentials has been illustrated by comparing results obtained with the Schwandt and the Madland potentials. At 150-MeV incident energy, the difference is barely noticeable, but it is significant at 175- and 200-MeV incident energies. Generally the shape of the angular distribution is preserved, but a renormalization of the value of V_0 between about 6 and 12 % is required at the highest incident energies (175 and 200 MeV). This effect should be taken into account when comparing effective interaction strengths derived using different optical potentials.

The first-step component of the MSD theory has been compared to the quasifree-knockout contribution based on a DWIA calculation, and a good correspondence between the two calculations was found. This lends further support to one of the assumptions underlying the statistical multistep direct theory, viz., that the initial stage of the cascade of nucleon-nucleon interactions initiated by the projectile can be interpreted in terms of a single inelastic nucleon-nucleon scattering.

On the whole, the results show that the angular distributions of the three targets investigated can be well described by the statistical multistep direct emission theory of Feshbach, Kerman, and Koonin, even up to the highest incident energy of 200 MeV.

[1] H. Gruppelaar, P. Nagel, and P. E. Hodgson, Riv. Nuovo Cimento **9**, 1 (1986).
[2] K. Chen, Z. Fraenkel, G. Friedlander, J. R. Grover, J. M. Miller, and Y. Shimamoto, Phys. Rev. **166**, 949 (1968); H. W. Bertini, G. D. Harp, and F. E. Bertrand, Phys. Rev. C **10**, 2472 (1974).
[3] H. Feshbach, A. Kerman, and S. Koonin, Ann. Phys. **125**, 429 (1980).
[4] R. Bonetti, M. B. Chadwick, P. E. Hodgson, B. V. Carlson, and M. S. Hussein, Phys. Rep. **202**, 171 (1991).
[5] J. M. Akkermans and A. J. Koning, Phys. Lett. B **234**, 417 (1990); A. J. Koning and J. M. Akkermans, Ann. Phys. **208**, 216 (1991).
[6] M. Trabandt, W. Scobel, M. Blann, B. A. Pohl, R. C. Byrd, C. C. Foster, and R. Bonetti, Phys. Rev. C **39**, 452 (1989).
[7] W. Scobel, M. Trabandt, M. Blann, B. A. Pohl, B. R. Remington, R. C. Byrd, C. C. Foster, R. Bonetti, C. Chiesa, and S. M. Grimes, Phys. Rev. C **41**, 2010 (1990).
[8] A. A. Cowley, A. van Kent, J. J. Lawrie, S. V. Förtsch, D. M. Whittal, J. V. Pilcher, F. D. Smit, W. A. Richter, R. Lindsay, I. J. van Heerden, R. Bonetti, and P. E. Hodgson, Phys. Rev. C **43**, 678 (1991).
[9] J. V. Pilcher, A. A. Cowley, D. M. Whittal, and J. J. Lawrie, Phys. Rev. C **40**, 1937 (1989).
[10] A. A. Cowley, S. V. Förtsch, J. J. Lawrie, D. M. Whittal, F. D. Smit, and J. V. Pilcher, Z. Phys. A **336**, 189 (1990).
[11] S. V. Förtsch, A. A. Cowley, J. J. Lawrie, D. M. Whittal, J. V. Pilcher, and F. D. Smit, Phys. Rev. C **43**, 691 (1991).
[12] P. Schwandt, H. O. Meyer, W. W. Jacobs, A. D. Bacher, S. E. Vigdor, M. D. Kaitchuck, and T. R. Donoghue, Phys. Rev. C **26**, 55 (1982).
[13] R. Bonetti, M. Camnasio, L. Colli Milazzo, and P. E. Hodgson, Phys. Rev. C **24**, 71 (1981).
[14] A. J. Koning and J. M. Akkermans (unpublished).
[15] E. Gadioli and P. E. Hodsgon, *Preequilibrium Nuclear Reactions* (Oxford University Press, New York, 1991), Chap. 7.
[16] H. Feshbach, Ann. Phys. **159**, 150 (1985).
[17] H. Feshbach (unpublished).
[18] R. Bonetti and C. Chiesa, MSD code, University of Milan (unpublished).
[19] P. D. Kunz, DWUCK4 code, University of Colorado (unpublished).
[20] D. G. Madland, Los Alamos National Laboratory Report LA-UR-87-3382.
[21] A. Bohr and B. R. Mottelson, *Nuclear Structure* (Benjamin, Reading, MA, 1969), Vol. I.
[22] A. V. Ignatyuk, G. N. Smirenkin, and A. S. Tishin, Yad. Fiz. **21**, 485 (1975) [Sov. J. Nucl. Phys. **21**, 255 (1975)].
[23] S. Shlomo and J. B. Natowitz, Phys. Lett. B **252**, 187 (1990).
[24] A. D'Arrigo, G. Giardina, and A. Taccone, Phys. Lett. B **262**, 1 (1991).
[25] M. B. Chadwick, Ph.D. thesis, Oxford University, 1989.
[26] P. E. Hodgson (unpublished).
[27] S. M. Austin, in *The (p,n) Reaction and the Nucleon-Nucleon Force,* edited by C. D. Goodman *et al.* (Plenum, New York, 1980), p. 203.
[28] Y. Holler, A. Kaminsky, R. Langkau, W. Scobel, M. Trabandt, and R. Bonetti, Nucl. Phys. **A442**, 79 (1985).
[29] E. Mordhorst, M. Trabandt, A. Kaminsky, H. Krause, W. Scobel, R. Bonetti, and F. Crespi, Phys. Rev. C **34**, 103 (1986).
[30] A. Marcinkowski, R. W. Finlay, J. Rapaport, P. E. Hodgson, and M. B. Chadwick, Nucl. Phys. **A501**, 1 (1989).
[31] M. B. Chadwick, P. E. Hodgson, and A. Marcinkowski (unpublished).